Journal of Catalysis 265 (2009) 199–208

Contents lists available at ScienceDirect

Journal of Catalysis

journal homepage: www.elsevier.com/locate/jcat

Kinetic study of CO desorption from PtRu/C PEM fuel cell anodes: Temperature dependence and associated microstructural transformations

A. Pitois *, J.C. Davies [1], A. Pilenga, A. Pfrang, G. Tsotridis

Institute for Energy, Joint Research Centre, European Commission, Postbus 2, 1755 ZG Petten, The Netherlands

ARTICLE INFO

Article history:
Received 28 January 2009
Revised 1 May 2009
Accepted 1 May 2009
Available online 29 May 2009

Keywords:
CO tolerance
Catalysis
Platinum
Ruthenium
Desorption
Isotope exchange
Temperature dependence
PEM fuel cell

ABSTRACT

The temperature dependence of the CO desorption process on a carbon-supported platinum–ruthenium alloy catalyst has been investigated using isotopic exchange experiments. The kinetics of CO desorption on PtRu/C catalyst have been studied as a function of temperature and flow rate. Desorption rate constants have been determined for a temperature range between 25 °C and 150 °C. All PtRu/C results have been compared with those obtained for the Pt/C catalyst under similar experimental conditions. Quite different desorption rate constants have been observed. The variation in apparent Arrhenius parameters (frequency factor A and activation energy E_a) for PtRu/C and Pt/C could possibly explain their different degrees of poisoning by CO in proton exchange membrane fuel cells (PEMFCs) and the underlying adsorption/desorption processes. The effect of temperature treatment on the PtRu/C catalyst properties has also been investigated with respect to CO desorption kinetics and to the associated microstructural transformations.

1. Introduction

Proton exchange membrane fuel cells (PEMFCs) are expected to achieve commercial application in a wide variety of areas including the automotive industry, because of having the inherent properties of high current density, being lightweight, operating at low temperatures, and containing no corrosive materials [1]. Platinum is currently the catalyst of choice for both the anode and cathode processes due to the high current densities obtained [2]. A possible source of hydrogen for the anode reaction is the reformation of hydrocarbons, by partial oxidation or steam reforming. This results in hydrogen containing, amongst other impurities, significant levels of CO. CO levels can be reduced down to ppm levels (by pressure swing adsorption or via the water gas shift reaction) but as little as 20 ppm CO is known to poison the platinum catalyst by blocking sites for hydrogen adsorption [3]. Platinum–ruthenium catalysts have attracted considerable interest in recent years as highly active and more CO tolerant anode catalysts in PEMFCs, both for the electrooxidation of CO-contaminated H_2-rich fuel gas and for the electrooxidation of methanol in direct methanol fuel cells [4,5]. Three possible effects have been identified to explain increased CO tolerance of platinum–ruthenium catalyst compared to pure platinum: the bifunctional mechanism, the ligand effect mechanism and the "detoxification" mechanism. The bifunctional mechanism suggests that the overpotential for CO oxidation to CO_2 is reduced by the presence of ruthenium through water dissociation at ruthenium, which is more facile than on Pt. This mechanism has been demonstrated extensively in the literature both theoretically [6–9] and experimentally [10–18]. Alternatively, the ligand effect mechanism suggests that combining platinum with ruthenium leads to a reduction in the Pt–CO bond strength, leading to a higher rate of CO oxidation at the surface. This mechanism has also been demonstrated both theoretically [6–9,19–22] and experimentally [15,22] but has been shown to have a less significant effect on the rate of CO oxidation than the bifunctional mechanism [24,25]. Similarly to the ligand effect mechanism, the "detoxification" mechanism involves a weakening of the Pt–CO bond strength due to the presence of ruthenium. However, in this case, this bond strength weakening is proposed to lead to a lower equilibrium CO coverage leaving more free sites for hydrogen oxidation [26,27].

Therefore, the issue of CO tolerance should be considered from the point of view of both the electrochemical CO oxidation and the equilibrium attained through the adsorption/desorption process, since the kinetically predominant of these two processes will govern the surface coverage of the CO species at steady-state. While the CO oxidation mechanisms, both bifunctional and ligand effect mechanisms, have been extensively investigated in the literature

* Corresponding author.
E-mail address: aurelien.pitois@ec.europa.eu (A. Pitois).
[1] Present address: Ilika Technologies Ltd., Kenneth Dibben House, Enterprise Road, University of Southampton Science Park, Chilworth, Southampton SO16 7NS, United Kingdom.

0021-9517/$ - see front matter © 2009 Elsevier Inc. All rights reserved.
doi:10.1016/j.jcat.2009.05.004

[6–23], only a few studies have been performed on the CO adsorption/desorption process [26,27]. The fundamental study of the CO adsorption/desorption process is, however, essential to better understand the CO poisoning behaviour on PEM fuel cell anodes.

In this study, CO isotope exchange experiments have been carried out to follow the CO desorption kinetics from supported PtRu to help understand the role of Ru in providing increased tolerance to CO in PEM fuel cells. CO isotope exchange experiments taking place at either the liquid–solid interface, in the electrochemical environment, or the gas–solid interface, were used in previous studies to help elucidate the mechanisms involved in CO tolerance at PEM fuel cell anodes. However, the actual environment within the fuel cell lies somewhere between these two conditions, as the supported catalyst is exposed to a humidified gas stream. CO exchange at the liquid–solid interface under the electrochemical environment was mainly studied using in situ infrared detection in an external reflection configuration [28–30]. Weaver et al. reported the infrared spectra for CO adsorbed at ordered Pt(1 1 1) aqueous interfaces for various $^{12}CO/^{13}CO$ mixtures [28,29]. Korzeniewski et al. probed qualitative structural features of the adlayers formed by CO at step sites and on terrace planes of Pt(3 3 5) and Pt(1 1 1) in the aqueous electrochemical environment [30]. They observed a site-dependent vibrational coupling of CO on the well-defined step and terrace sites on monocrystalline Pt. Lately, they studied the isothermal desorption of CO from a polycrystalline Pt electrode using an infrared spectroelectrochemical cell capable of operating at temperatures between ambient and 70 °C and found solvent influences upon CO adlayer stability [31,32]. CO exchange at the gas–solid interface was studied by monitoring the changes in the adlayers on Pt(1 1 1) by infrared spectroscopy and by following the desorption of ^{13}CO from carbon-supported Pt and PtRu catalysts by mass spectrometry [33–35]. Andersen et al. used infrared spectroscopy to investigate the CO desorption rate dependence on CO partial pressure over a Pt(1 1 1) single crystal [33]. Davies et al. performed similar experiments over supported commercial Pt and PtRu fuel cell catalyst [34,35]. They found that the rates of desorption for equivalent partial pressures are many orders of magnitude higher for the single crystal surface than for the nanoparticulate catalysts. This was attributed to the facets of the nanoparticles being considerably smaller than the unit cell obtained on Pt(1 1 1), hereby quantising the coverages obtained on these facets at coverages at which the CO is more strongly bound. The CO exchange rates measured at room temperature and under dry conditions for a CO concentration of 100 ppm in argon or hydrogen on both Pt/C and PtRu/C are, however, considered as high compared to the equivalent electrochemical CO oxidation rate measured under the operating conditions of the fuel cell, suggesting that the adsorption/desorption process may have a significant influence with regard to the poisoning effect of CO on the PEM fuel cell anode [34,35]. It has, however, to be noted that these investigations were not performed under electrochemical conditions. Recently Behm et al. investigated on a Pt electrode the room temperature desorption and exchange of CO in a saturated CO adlayer at potentials far below the onset of oxidation by isotope CO exchange experiments using a novel set-up for the simultaneous in situ IR spectroscopic and online mass spectrometric detection of adsorbed species under controlled mass transport conditions [36]. They reported that adsorbed CO exchanges rapidly under these experimental conditions. This fast exchange was attributed to a decrease in the desorption barrier, caused by a combination of two effects: a slight increase in adsorbed CO coverage upon increasing the CO pressure and a pronounced decay of the CO adsorption energy with coverage, due to lateral repulsive $CO_{adsorbed}$–$CO_{adsorbed}$ interactions.

The aim of the present work is to investigate for a real industrial catalyst the effect of increasing temperature on the CO exchange rate over a range that is of relevance to the operating PEM fuel cell. Currently, the research community is engaged in the development of new membranes for the PEM fuel cell capable of operating at higher temperatures than the current industry standard, the Nafion membrane, which is limited by its need for humidification by water to less than 100 °C. Therefore, a temperature range between 25 °C and 150 °C has been used for the measurements. The temperature-dependent kinetics of CO desorption from Pt/C catalyst have been recently investigated by Davies et al. [27] and the measured rates of desorption are high compared with the rates of oxidation measured from polarisation curves obtained with high concentrations of CO in argon [13]. However, the CO exchange rate on the PtRu/C catalyst at temperatures above room temperature has not previously been investigated. So there is a need to determine whether the CO oxidation mechanism or the CO adsorption/desorption process has a greater influence on the steady-state CO coverage and consequently the CO tolerance of the PtRu catalyst.

In this study, data have been obtained for a temperature range of 25 to 150 °C for a current industrial PtRu/C system. The kinetics of CO desorption on PtRu/C catalyst were investigated as a function of the temperature and the flow rate. Desorption rate constants were deduced from the CO desorption kinetics data and the results were compared with those previously published for Pt/C under similar conditions [27]. The apparent Arrhenius parameters, both the frequency factor A and the activation energy E_a, were also deduced from the temperature-dependent kinetic study of CO desorption for both PtRu/C and Pt/C and results were compared. Finally, the effect of temperature treatment on the properties of the PtRu/C catalyst was investigated studying the kinetics of CO desorption on an "already tested" sample, and associated microstructural transformations were characterised by X-ray diffraction and microscopy techniques such as Scanning Electron Microscopy (SEM) and Transmission Electron Microscopy (TEM).

2. Material and methods

2.1. Material

Commercial PtRu catalysts from Electrochem Inc. supported on Vulcan carbon XC72 and bound to Toray carbon paper diffusion layers with a Teflon binder were used for the CO desorption kinetics experiments. The catalyst loading was 1 mg/cm^2 Pt (20 wt%) and 0.5 mg/cm^2 Ru (10 wt%). Contrary to the Nafion binder, which enables experiments only below 100 °C for water management reasons, a Teflon binder ensures the ability to perform experiments at higher temperatures (up to 150 °C in this study). All gases used (argon, hydrogen, 1000 ppm ^{12}CO in argon mixture and 1% ^{13}CO in argon mixture) were obtained from Linde and were of the highest commercially available purity. For the 1% ^{13}CO in argon gas mixture, the CO has been enriched to the ratio 99% ^{13}CO/1% ^{12}CO.

2.2. Methods

2.2.1. CO desorption kinetics

CO desorption kinetics experiments have been performed using a flow cell based on a conflate design in a flow mode. Circular catalyst samples of diameter 3.6 cm were used in the flow cell. A gas dosing system allowed a fast interchange between various gases. The intrinsic delay of the system when switching gases has been demonstrated as having negligible effects on the experiments for the conditions used and there is no significant increase in the cell pressure due to the resistance of the cell/sample, when the flow rate is varied [27]. The gas was extracted from the cell via a quartz tube sniffer and both its content and composition were measured in "real time" using a quadrupole mass spectrometer. The flow cell

temperature was set using an oven. The experimental setup used for the study as well as a cross-sectional view of the flow cell is given in Fig. 1.

The following procedure was applied to determine the CO desorption kinetics. The catalyst surface was initially saturated by isotopically labelled ^{13}CO at a given temperature using a 1% ^{13}CO in argon gas mixture in order to completely cover the catalyst surface with ^{13}CO. The residual ^{13}CO was then removed from the flow cell using argon. In order to obtain the desorption profile for ^{13}CO, natural ^{12}CO at a concentration of 1000ppm in argon was allowed to flow through the cell, and mass 29 corresponding to ^{13}CO was measured by a mass spectrometer. The complete experimental procedure for the CO desorption kinetic study is summarised in Table 1.

This procedure, close to a Steady-State Isotopic Transient Kinetic Analysis (SSITKA) procedure, was already used successfully for similar studies [27,34] and has the advantage to reduce the required time for each data point compared to SSITKA. This

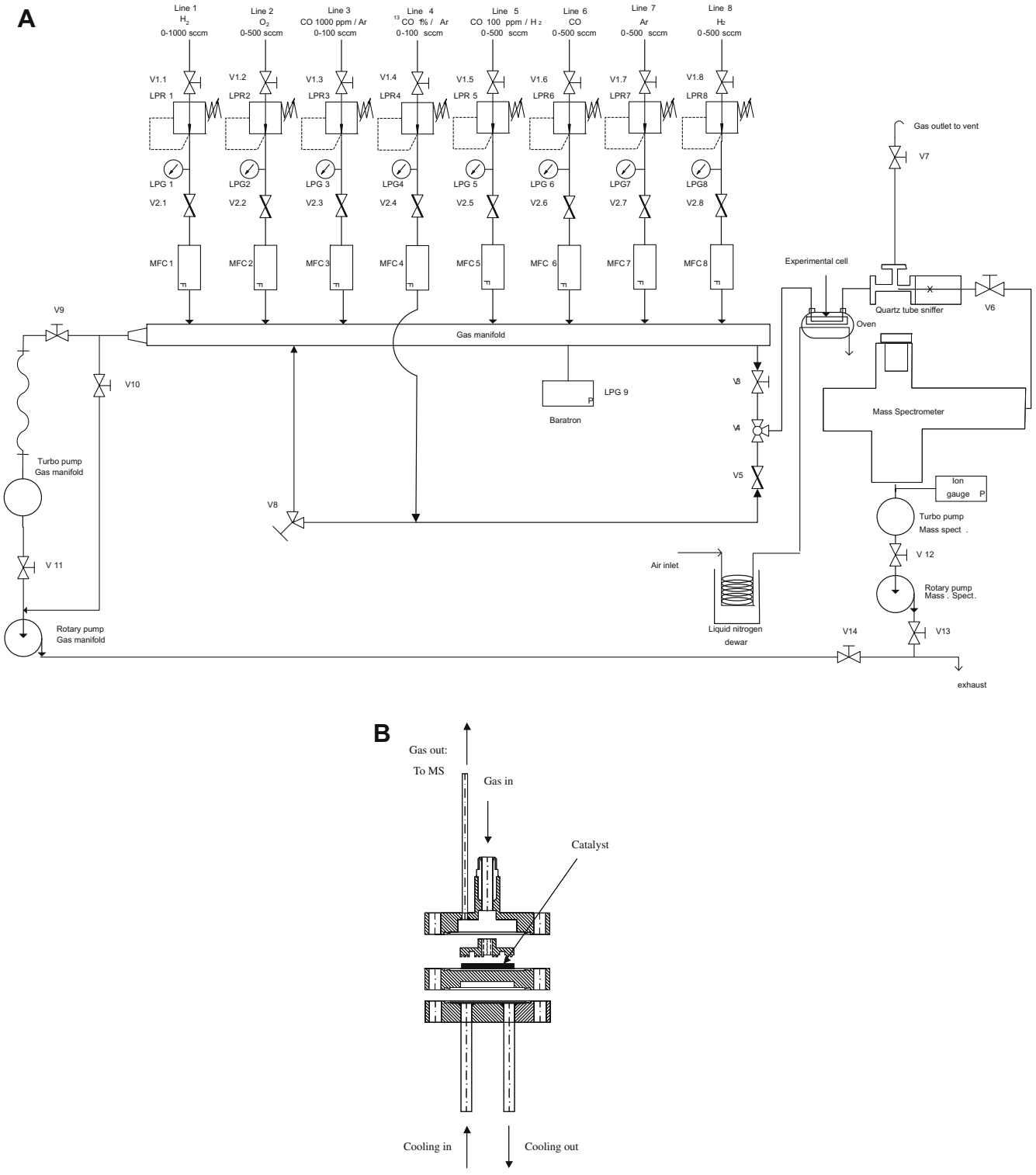

Fig. 1. (A) Experimental setup used for the kinetic study of CO desorption. (B) Cross-section of the flow cell.

Table 1
Experimental procedure for the CO desorption kinetic study.

Step	Duration (min)	Procedure	Aim
1	30	Stream of H_2	Cleaning of the catalyst surface
2	30	Stream of Ar	Removal of residual H_2
3	30	Stream of labelled ^{13}CO at a given temperature	Saturation of the catalyst surface with ^{13}CO
4	30	Stream of Ar	Removal of residual ^{13}CO
5	At least 180 min	Stream of natural ^{12}CO at a given temperature and flow rate	Measurement of the ^{13}CO desorption kinetics
6	Overnight	Stream of Ar	Catalyst surface in an inert gas

procedure was performed for a wide range of temperatures (25 °C, 50 °C, 75 °C, 100 °C, 125 °C and 150 °C) and flow rates (30 ml/min, 60 ml/min, 90 ml/min, 120 ml/min and 135 ml/min). To assess the effect of temperature treatment on the catalyst properties, the PtRu catalyst, which underwent the procedure for all temperatures and flow rates, was used once again to repeat the initial CO desorption kinetics experiment (temperature: 25 °C and flow rate: 30 ml/min). Results obtained for this "already tested" catalyst were recorded and compared with the initial data. Microstructural characterisations of the PtRu/C catalyst, before and after temperature treatment, were performed by X-ray diffraction (XRD), Scanning Electron Microscopy (SEM) and Transmission Electron Microscopy (TEM) in order to investigate the microstructural transformations associated to the temperature treatment.

2.2.2. X-ray diffraction

Characterisation of the PtRu/C catalysts, both before and after temperature treatment, was performed using a Philips PW 3830 X-ray diffraction apparatus. The average catalyst particle size was obtained using the Debye–Scherrer broadening of X-ray diffraction data.

2.2.3. Scanning Electron Microscopy

The microstructure of the PtRu/C catalysts, both before and after temperature treatment, was investigated using a Zeiss Supra 50 Field-Emission Gun Scanning Electron Microscope. Changes in the microstructure of the catalyst and support combination due to temperature treatment were assessed. An Oxford Gemini EDX detector was associated to the Scanning Electron Microscope.

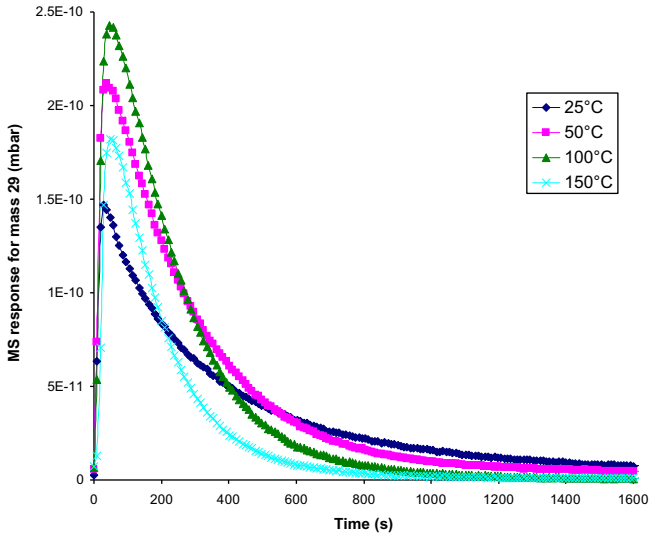

Fig. 2. Mass spectrometer traces for mass 29 (^{13}CO) on switching to 1000 ppm ^{12}CO in argon for various temperatures (25 °C, 50 °C, 100 °C and 150 °C) at a fixed flow rate of 90 ml/min.

2.2.4. Transmission Electron Microscopy

Materials scraped from the catalyst layer of tested and untested samples were characterised using a FEI Tecnai 20 Transmission Electron Microscope operated at 200 kV with a LaB_6 filament. The degree of aggregation of catalyst particles due to temperature treatment was assessed.

3. Results and discussion

3.1. Kinetic study of the CO desorption from PtRu/C catalyst

The desorption kinetics of adsorbed isotopically labelled ^{13}CO in the presence of natural ^{12}CO at 1000 ppm in the gas phase were studied as a function of the temperature (25 to 150 °C) and flow rate (30 to 135 ml/min). The relationships between the ^{13}CO desorption profile and the kinetics of the desorption process are explained in detail elsewhere [27].

3.1.1. Influence of the temperature

Mass spectrometer traces for mass 29 (^{13}CO) on switching to 1000 ppm ^{12}CO in argon are shown in Fig. 2 for various temperatures (25 °C, 50 °C, 100 °C and 150 °C) at a fixed flow rate of 90 ml/min.

From the CO desorption profiles shown in Fig. 2, it can be observed that the CO desorption kinetics from PtRu/C catalyst increase with temperature across the temperature range investigated, and that the area under the exchange curve decreases with temperature. This behaviour is similar to that observed by Davies et al. for a Pt/C catalyst under similar experimental conditions [27].

Assuming that at infinite time all CO will have exchanged, the relative CO coverage can be obtained from the area under the ^{13}CO desorption curves. The relative coverage values versus temperature for the data obtained at a fixed flow of 90 ml/min are given in Fig. 3. All data have been normalised against a value of 1 for

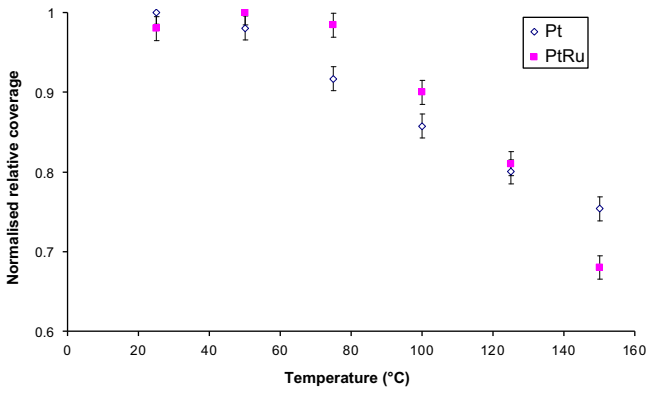

Fig. 3. Normalised relative coverage value for Pt [27] and PtRu catalysts versus temperature. Values for both Pt and PtRu catalysts have been obtained under similar experimental conditions (^{13}CO peak area for exchange at 1000 ppm CO in Ar at a flow rate of 90 ml/min).

the highest area under the ^{13}CO desorption curve, thus giving a relative, rather than an absolute coverage. Normalised relative coverage values for pure platinum are also given for comparison.

As expected, the relative CO coverage on the PtRu/C catalyst decreases with increasing temperature. This trend is similar to that observed in a previous study for the Pt catalyst under similar experimental conditions [27] and can be correlated to the CO desorption data obtained by Temperature-Programmed Desorption (TPD) for both Pt and PtRu [37]. However, whereas the relative CO coverage for Pt is 1 only at 25 °C, the relative coverage for PtRu is not significantly different from 1 for temperatures up to 75 °C. The maximum relative coverage is thus kept for a larger temperature range for the PtRu catalyst compared to the Pt catalyst. After their maximum, the relative coverage then decreases in both cases. However, the decrease rate for the relative CO coverage is faster on PtRu than on Pt: whereas the linear decrease in relative coverage per degree Celsius is 2.3×10^{-3} between 50 °C and 150 °C for the Pt catalyst, this value is 4.0×10^{-3} for the PtRu catalyst between 75 °C and 150 °C, indicating a much stronger decrease in relative coverage with temperature for PtRu compared to Pt. It has, however, to be pointed out that the initial absolute coverage (per surface atom) of CO is lower on PtRu than on Pt [16] and that these observations concern only the relative change in CO surface coverage for the Pt and PtRu catalyst surfaces as a function of temperature.

3.1.2. Influence of the flow rate

The flow-rate dependence of the CO exchange is shown in Fig. 4 for flow rates ranging from 30 ml/min to 135 ml/min and a fixed temperature of 50 °C.

There is a clear flow-rate dependence of the measured desorption rate. The flow-rate dependence increases with increasing temperature. This phenomenon, already observed in a previous study [27], occurs when there is a significant readsorption of ^{13}CO during the desorption experiments due to high concentration of desorbed species above the sample surface during the experiments. This readsorption can be related to the catalyst accessibility for the exchange. For the thick catalyst layers the exchange occurs at a high rate at the outer layer, whereas an internal diffusion within the catalyst layer occurs. Thus the exchanged CO can re-adsorb before leaving the catalyst bed. As a consequence only an apparent rate of desorption, lower than the actual rate, can be observed.

3.1.3. Determination of the desorption rate constant

Using a method similar to Xu et al. [38] and assuming pseudo-steady-state conditions, the decay curve for the ^{13}CO concentration can be written in the form

$$C = \frac{\theta_{CO} k^-}{q + \frac{\theta_{CO} k^-}{C_0}} \exp\left[-\frac{k^-}{1 + \frac{\theta_{CO} k^-}{q C_0}} t\right] \quad (1)$$

where C is the ^{13}CO concentration at time t, C_0 is the initial ^{13}CO concentration, q is the flow rate, θ_{CO} is the coverage and k^- is the desorption rate constant.

Therefore, the initial gradient of the semilogarithmic plot could be defined as an apparent rate of desorption $k_{apparent}$ (dependent on the flow rate):

$$k_{apparent} = \frac{k^-}{1 + \frac{\theta_{CO} k^-}{q C_0}} \quad (2)$$

The previous equation can be rewritten in the following way to provide the determination of the desorption rate constant:

$$\frac{1}{k_{apparent}} = \frac{1}{k^-} + \frac{\theta_{CO}}{C_0} \frac{1}{q} \quad (3)$$

And so a plot of $1/k_{apparent}$ versus $1/q$ should provide a linear response, with an intercept of $1/k^-$, k^- being the desorption rate constant.

This plot is given in Fig. 5 for the determination of the desorption rate constant for PtRu/C catalyst at various temperatures. Data obtained for the Pt/C catalyst are also given for comparison.

The desorption rate constants k^- for the PtRu catalyst are given as a function of the temperature in Table 2. The rate constants for the Pt catalyst are also given in Table 2 for comparison.

Comparing the sets of data for the Pt and PtRu catalysts, it is immediately evident that within the confines of our experimental arrangement it is possible to obtain measurements of the rate of desorption up to 150 °C on PtRu, as the rates of exchange increase at a far more gradual rate on PtRu with increasing temperature than on Pt where it was no longer possible to extract any kinetic information above 75 °C. However, it should also be noted that the desorption rate at room temperature is initially higher on PtRu than on pure Pt.

In order to compare the kinetics of the CO desorption and electrochemical CO oxidation processes, the PtRu desorption rate constants can be converted to equivalent CO oxidation current densities. Assuming the number of Pt sites per cm^2 to be 1.50×10^{15} (close-packed Pt(1 1 1)) and that two electrons are oxidised per CO molecule, equivalent CO oxidation current densities range from 15 μA cm^{-2} at 25 °C to 960 μA cm^{-2} at 150 °C. These equivalent CO oxidation current densities are high when compared with the rates of oxidation measured from polarisation curves obtained with high concentrations of CO in argon [13]. For example, the equivalent current density for the CO electrooxidation on PtRu for 2% CO in argon at 62 °C would require an overpotential equal to 0.55 V [13]. This significant overpotential is not observed as a

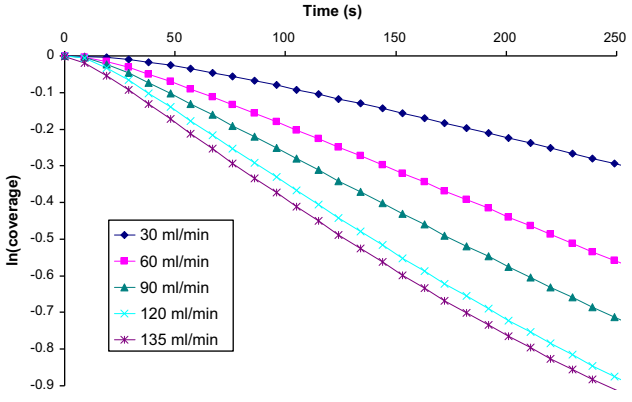

Fig. 4. Flow-rate dependence of the CO exchange at 50 °C.

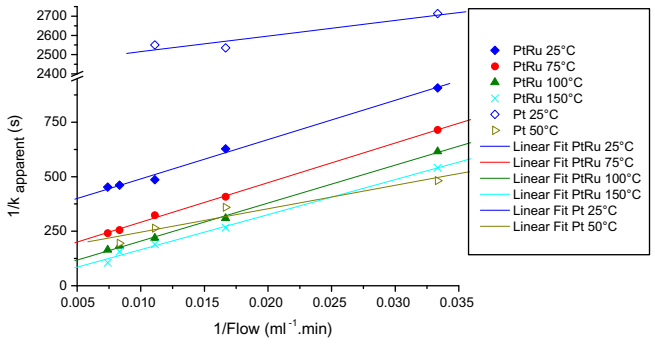

Fig. 5. Determination of the desorption rate constant for PtRu catalyst at various temperatures, by plotting the $1/k_{apparent}$ versus the inverse flow rate. Data for Pt catalyst are given for comparison.

Table 2
Desorption rate constant k^- for PtRu and Pt catalysts, respectively, as a function of the temperature. The uncertainty on the values is 4%.

Temperature (°C)	k^-_{PtRu} (s^{-1})	k^-_{Pt} (s^{-1}) [27]
25	3.2×10^{-3}	4.0×10^{-4}
50	8.9×10^{-3}	2.5×10^{-2}
75	2.2×10^{-2}	1.1×10^{-1}
100	3.3×10^{-2}	$>3 \times 10^{-1}$
125	6.4×10^{-2}	$>3 \times 10^{-1}$
150	2.0×10^{-1}	$>3 \times 10^{-1}$

potential loss for the fuel cells operating at that temperature. This would suggest that in the fuel cell environment it is the adsorption/desorption equilibrium that has the greater influence on the equilibrium CO coverage: the adsorption/desorption process would be kinetically predominant compared to the electrochemical CO oxidation. This would imply that in the fuel cell environment the "detoxification" mechanism would be the major mechanism to explain the CO tolerance. However, it must be stressed that the experiments performed in this study do not contain humidification or a potential field and therefore provide a simplified adsorption environment. These effects are expected to play an important role in the balance between desorption and CO oxidation via the bifunctional mechanism within the operating fuel cell environment. Density Functional Theory (DFT) calculations showed that raising the potential leads to an increase in the rate of hydrogen adsorption, water dissociation, CO oxidation and hydrogen oxidation because of the strong potential-dependence of the reactions [39]. In general it is agreed that the addition of Ru to Pt reduces the overpotential for CO oxidation, i.e. there is a proven bifunctional effect of combining these two metals. It is widely accepted that this promotional effect stems from the greater ease by which Ru dissociates water compared to Pt and is not primarily due to a reduction in the CO bond strength. Christensen et al. suggested from in situ infrared spectroscopy studies that adsorbed CO on both the Ru and Pt domains is oxidised by the oxygen-containing adlayer on the Ru in a chemical process to produce CO_2 and that there is a free exchange of $CO_{adsorbed}$ between the Ru and Pt sites [40]. However, the most relevant current issue over which there is still significant debate is whether this is the dominant process governing the promotional behaviour considering the low potential drop experienced across fuel cell anodes. Whilst studies have shown that at higher potentials [41] significant oxidation occurs, it is not so clear at lower potentials. It has been demonstrated that to give effective CO tolerance only nanoamps of CO oxidation currents may be required. Hence at lower potentials such as those at fuel cell anodes the alternative process of an electronic effect modifying the process should be considered. Koper et al. found using DFT calculations that mixing of Pt to Ru weakens the binding of both CO and OH to the Pt surface sites, whereas mixing of Ru to Pt causes a stronger binding of CO and OH to the Ru surface sites [42]. Therefore, within fuel cell operating conditions (humidified gas stream, oxidative and open circuit conditions), a decrease in the steady-state CO coverage, which would be a driving force for the CO exchange, may be expected on the PtRu catalyst. Norskov et al. found that the promoting effect of Ru for Pt anodes is due to both the ligand effect and the bifunctional effect for the CO oxidation process, but that the dominating effect is the ligand effect/"detoxification" mechanism for the PEM fuel cell [39].

It is also worth noticing that it may be also the case for Pt since recently it was observed by Behm et al. [36] that CO exchanges rapidly on a Pt electrode compared to the extremely low CO adsorbed oxidation under electrochemical conditions, at potentials in the H-upd region and at room temperature. Comparing their results for CO isotope exchange experiments under electrochemical environment with results from gas phase isotope exchange experiments on supported Pt catalyst [34], Behm et al. found that the presence of the electrolyte and the applied potential do not cause a significant stabilisation of the adlayer against exchange [36]. Therefore, they suggested that, at a typical PEMFC operation temperature of 80 °C, $CO_{adsorbed}$ desorption will be sufficiently fast in an electrochemical environment that it can contribute significantly to keep the steady-state $CO_{adsorbed}$ coverage at tolerable levels even in contact with CO-contaminated feed gas, if the CO concentration is not too high.

The modification of the current setup aiming at progressing from the current simplified adsorption system to more accurately representing the real fuel cell environment is being performed in order to follow the temperature dependence of the CO desorption kinetics from supported PtRu in real fuel cell conditions.

3.1.4. Determination of the apparent Arrhenius parameters

The temperature dependence of the desorption rate constant is given by the Arrhenius equation as shown below

$$k = A \cdot e^{-E_a/RT} \tag{4}$$

where k is the rate constant in s^{-1}, A is the frequency factor in s^{-1}, E_a is the activation energy in J mol^{-1}, R is the gas constant and T is the temperature in K. The frequency factor can be considered as independent of temperature and hence a constant.

Taking the natural logarithm of the Arrhenius equation yields the following relationship:

$$\ln(k) = \frac{-E_a}{R}\frac{1}{T} + \ln(A) \tag{5}$$

So, plotting the logarithmic value of the desorption rate constant versus the inverse temperature should give a straight line, whose slope and intercept can be used to determine the activation energy E_a and the frequency factor A. In our case, since the desorption process does not correspond to an elementary step, only apparent Arrhenius parameters (frequency factor A and activation energy) can be obtained. The apparent Arrhenius parameters have been determined for PtRu and Pt catalysts, respectively, using the Arrhenius equation and the temperature-dependent CO desorption data. The Arrhenius plots as well as the apparent Arrhenius parameters for the PtRu and Pt catalysts are given in Fig. 6 and in Table 3, respectively.

The PtRu and Pt catalysts show strongly contrasting parameters for the CO desorption process. The Pt catalyst presents a much higher value for the apparent frequency factor A ($A = 5.7 \times 10^{13}$ s^{-1}) than the PtRu catalyst ($A = 1.9 \times 10^{3}$ s^{-1}). On the contrary, the PtRu catalyst has a lower apparent activation energy than the

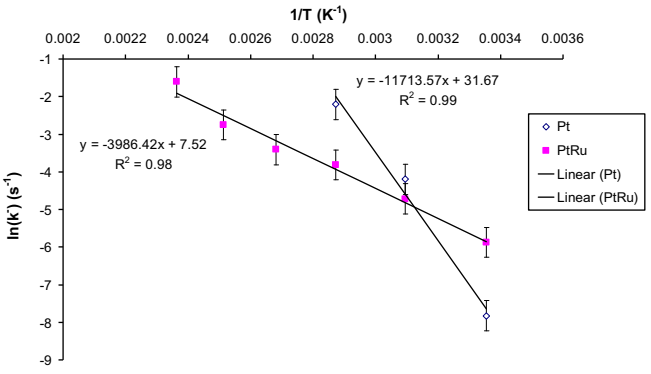

Fig. 6. Determination of the apparent Arrhenius parameters for the PtRu and Pt catalysts using the Arrhenius plot (logarithmic value of the desorption rate constant versus the inverse temperature).

Table 3
Apparent Arrhenius parameters (apparent frequency factor A and apparent activation energy E_a) for PtRu and Pt catalysts, respectively.

Catalyst	Apparent frequency factor A (s^{-1})	Apparent activation energy E_a (kJ mol^{-1})
Pt	5.7×10^{13}	97.4
PtRu	1.9×10^{3}	33.2

Pt catalyst for the CO desorption process (97.4 kJ mol^{-1} and 33.2 kJ mol^{-1} for Pt and PtRu, respectively). The calculated apparent frequency factor value for the Pt catalyst is in good agreement with the value of 10^{13} s^{-1} usually used in the literature [27,34]. To our knowledge, no frequency factor value for the PtRu catalyst has been experimentally reported yet in the literature; however, the calculated apparent frequency factor is in the same order of magnitude as the expected ones for the desorption process of gases on metal alloy surfaces [43]. The apparent activation energies for the CO desorption process, calculated for both the Pt and PtRu catalysts, are in good agreement with those determined in the literature. In previous studies, which were concerned with investigating the replacement of ^{13}CO preadsorbed by gaseous ^{12}CO on polycrystalline platinum [44], a dependence on temperature was observed and a value of 90 kJ mol^{-1} for the activation energy was obtained for the desorption process. From the higher CO tolerance of the PtRu alloy compared to pure Pt, a lower activation energy is obviously expected for the PtRu catalyst. However, further analysis coupled to Temperature-Programmed Desorption (TPD) experiments is necessary. Effects such as intrinsic particle size effect [45] and coverage effect [24] probably account for the strongly contrasting Pt and PtRu behaviours in terms of Arrhenius parameters. It has to be pointed out that the particle size, the nature of the sites available for CO adsorption as well as the lateral repulsive $CO_{adsorbed}$-$CO_{adsorbed}$ interactions onto these two surfaces are strongly different. As determined using the Debye–Scherrer broadening of X-ray diffraction data shown below, the particle size of the PtRu catalyst (4.4 nm) is smaller than that of the Pt catalyst (6.0 nm). In addition to the fact that the CO adsorption bond is weaker on Ru than on Pt as indicated by nuclear magnetic resonance (NMR) results [46], stronger binding of CO on smaller particles was found using electrochemical NMR spectroscopy methods [46–50]. It has been explained by an increase in the Pt Fermi level local density of states: the proportion of edge CO binding sites versus terrace sites increases for the smaller particles. Thus decreasing particle size causes drastic changes in terms of the relative population of available CO adsorption sites, the CO adsorption energy varying with the variety of sites, i.e. edges and terraces [49]. The infrared characterisation of size-dependent nanoparticles by using chemisorbed CO as a structural probe indicated also a sharply increasing proportion of edge versus terrace Pt sites for particle diameter below 5 nm [50]. The Arrhenius parameters are also known to strongly vary with coverage on metal surfaces due to lateral repulsive interactions between CO molecules leading to a weakening of the M–CO bond and these are clearly very different on these two surfaces. It has been previously observed that the initial absolute coverage (per surface atom) of CO is reduced on PtRu surfaces compared to pure Pt [16] and it has been shown previously in this study that the rate of decrease in the relative CO coverage with temperature is larger on PtRu than on Pt. Thus a strong coverage effect is expected.

3.2. Effect of temperature treatment on the PtRu/C catalyst properties

The effect of temperature treatment on the PtRu/C catalyst properties has been investigated with regard to the CO desorption kinetics and the associated microstructural transformations.

3.2.1. Effect on the CO desorption kinetics

The PtRu/C catalyst, which had been used previously for the temperature-dependent CO desorption experiments and had consequently already undergone a cycle of experiments up to 150 °C, has been used once again for CO desorption experiments at 25 °C. The CO desorption profiles for the PtRu/C catalyst, respectively, before and after the thermal treatment, are presented in Fig. 7A for a temperature of 25 °C and a fixed flow rate of 90 ml/min.

There is a difference in behaviour between the CO desorption kinetics of the PtRu/C catalyst before and after thermal treatment. The CO desorption kinetics are faster after the temperature treatment, indicating some changes in the PtRu/C catalyst properties due to the thermal treatment. The relative coverage is, however, not significantly affected by the thermal treatment. The desorption rate constant for the PtRu/C catalyst after thermal treatment has been calculated and has been compared to that obtained for the original PtRu/C catalyst. The plot enabling the determination of the desorption rate constant of the PtRu/C catalyst, before and after thermal treatment, at 25 °C is shown in Fig. 7B.

A desorption rate constant of 8.0×10^{-3} s^{-1} has been found for the PtRu/C catalyst after thermal treatment. This value is higher by a factor 2 than that obtained for the original PtRu/C catalyst for a temperature of 25 °C before thermal treatment ($k^{-} = 3.2 \times 10^{-3}$ s^{-1}).

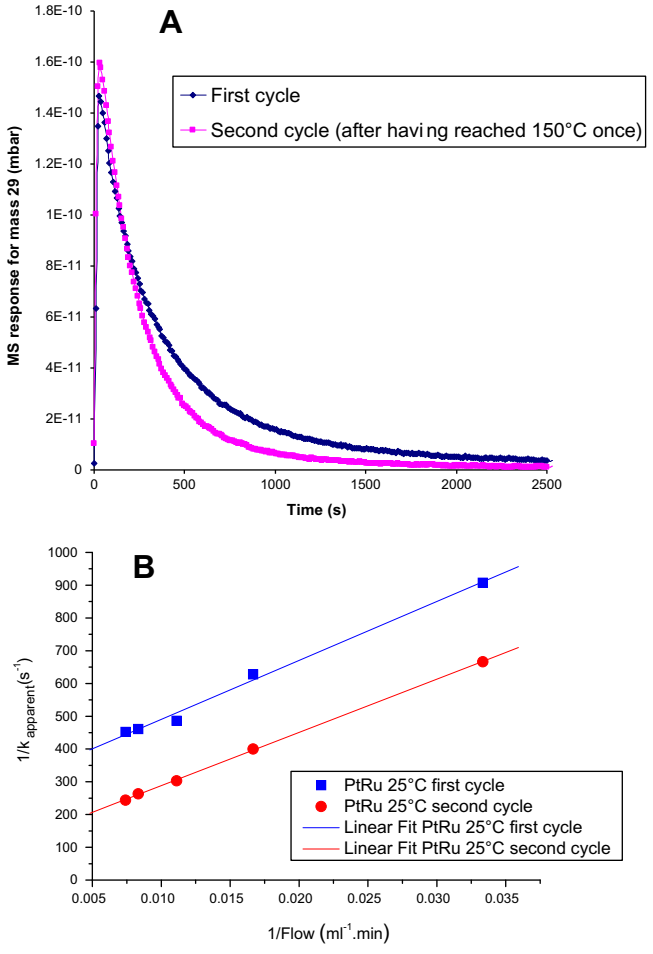

Fig. 7. (A) Effect of temperature treatment on the PtRu catalyst: CO exchange data at 25 °C and at a 90 ml/min flow rate, with original catalyst and catalyst having undergone a cycle of experiments up to 150 °C. (B) Effect of temperature treatment on the desorption rate of original and temperature-treated PtRu catalyst at 25 °C.

In an attempt to explain the slightly different behaviour of the PtRu/C catalyst after thermal treatment regarding the CO desorption kinetics, a microstructural characterisation of the PtRu/C catalyst, before and after thermal treatment, has been performed.

3.2.2. Associated microstructural transformations

X-ray diffraction, scanning electron microscopy and transmission electron microscopy have been used to investigate the microstructural transformations associated with the temperature treatment of the catalyst.

3.2.3. X-ray diffraction

The X-ray diffraction patterns for the PtRu/C catalyst, before and after temperature treatment, are shown in Fig. 8.

The peak located at a 2θ value of about 54° in the XRD pattern is referred to the carbon support. The other four peaks are characteristic of face-centred cubic (fcc) crystalline Pt, corresponding to the planes (1 1 1), (2 0 0), (2 2 0) and (3 1 1), respectively, indicating that the alloy catalyst has single-phase-disordered structures. The diffraction peaks for the PtRu/C catalyst are slightly shifted to higher 2θ values, when compared to the 2θ values of pure Pt given by the Joint Committee on Powder Diffraction Data [51], revealing the formation of an alloy involving the incorporation of Ru atoms into the fcc structure of Pt. The average particle size has been estimated from the Pt(1 1 1) full width at half-maximum (FWHM) according to the Debye–Scherrer formula. A similar average particle size of 4.4 nm has been found for the PtRu/C catalyst, before and after temperature treatment, indicating on average no change in the catalyst particle size due to temperature treatment. It has, however, to be considered that the average size as determined by XRD corresponds to the size of coherent domains and not necessarily to the size of particles, which either have an amorphous shell or are agglomerates of smaller, differently oriented particles. Therefore complementary Transmission Electron Microscopy images may be helpful in determining the change in catalyst active surface area even if the number of particles analysed by TEM is limited and – due to the two-dimensional nature of the data – overlapping particles might be interpreted as one larger particle. Consequently, a combination of both methods – XRD and TEM – seems appropriate.

3.2.4. Scanning Electron Microscopy and EDX spectrum

Scanning electron micrographs of the PtRu/C catalyst surface, before and after temperature treatment, are shown at different magnifications in Fig. 9A–C. Additionally, an EDX spectrum characteristic of the PtRu/C catalyst surface is presented in Fig. 9D.

Presence of micrometer level cracks is observed on the SEM image of the PtRu/C catalyst after temperature treatment at low magnification (×200). These cracks may be present in the binder due to temperature treatment, since the PtRu catalyst is bound to the carbon support by a Teflon binder. The catalyst surface structure obtained at high magnification (×50000) is, however, similar for both the PtRu/C catalysts, before and after temperature treatment. The EDX spectrum reflects the incorporation of ruthenium into the platinum structure for the carbon-supported PtRu catalyst.

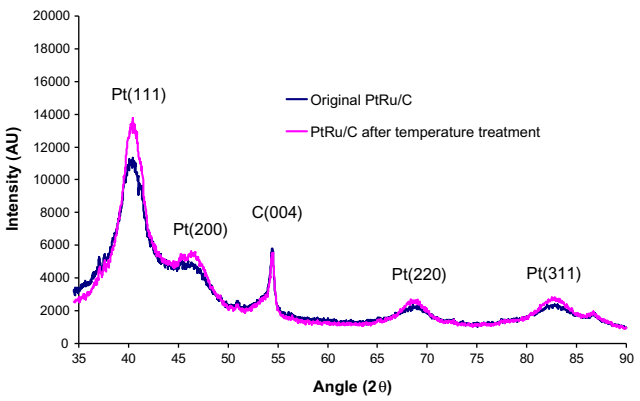

Fig. 8. X-ray diffraction patterns of the PtRu/C catalyst, before and after temperature treatment.

3.2.5. Transmission Electron Microscopy

Transmission electron micrographs of PtRu catalyst single particles observed at a ×230000 magnification, before and after temperature treatment, are presented in Fig. 10A and B. The atomic structure of the PtRu catalyst nanoparticle observed at a ×880000 magnification is also shown in Fig. 10C.

The PtRu catalyst nanoparticles appear to be finely dispersed on the carbon support. This high dispersion of the catalyst nanoparticles is an evidence of its high surface area and consequent high activity regarding the hydrogen oxidation reaction. The size of the catalyst nanoparticle observed by TEM (Fig. 10A) is in good agreement with the average particle size of 4.4 nm found by XRD. Some aggregation of catalyst nanoparticles may be observed after temperature treatment as shown in Fig. 10B. This phenomenon is, however, rare and cannot be generalised to the whole sample surface. It has also to be kept in mind that TEM analyses offer images of very specific locations of the sample surface and that in average no change in the catalyst particle size, before and after temperature treatment, has been observed by XRD. A possible mechanism for the local agglomeration of catalyst particles on the carbon support would be cluster–cluster coalescence at the nanometer scale [52]. At the highest magnification (×880000) the atomic structure of the PtRu catalyst single particle can be observed as shown in Fig. 10C.

4. Conclusions

The temperature-dependent kinetics of CO desorption on commercial PtRu/C fuel cell catalysts have been determined from CO isotope exchange experiments for 1000 ppm CO in Ar. Desorption rate constants have been obtained for temperatures ranging from 25 °C to 150 °C. These rates appear to be significantly higher than previously published CO oxidation rates obtained at similar concentrations and temperatures. This would imply that the adsorption/desorption equilibrium has the greater influence on the equilibrium CO coverage in the fuel cell environment. It must, however, be stressed that the experiments performed in this study do not contain humidification or a potential field and therefore provide a simplified adsorption environment. These effects are expected to play an important role in the balance between desorption and CO oxidation via the bifunctional mechanism within the operating fuel cell environment. Therefore, future studies will attempt to progress from the current simplified adsorption system to more accurately represent the real fuel cell environment. The apparent Arrhenius parameters, both the frequency factor A and the activation energy E_a, have been calculated for both PtRu/C and Pt/C catalysts. The variations in apparent Arrhenius parameters for PtRu/C and Pt/C, respectively, may explain their different CO poisoning effect and the underlying adsorption/desorption processes. A particle size effect or a coverage effect may account for the different behaviours between the Pt and PtRu catalysts.

The effect of temperature treatment on the PtRu/C catalyst properties has been investigated with regard to the CO desorption kinetics and to the associated microstructural transformations. The slightly different behaviour of the PtRu/C catalyst after thermal treatment regarding the CO desorption kinetics may be explained to some extent by a local aggregation of catalyst nanoparticles.

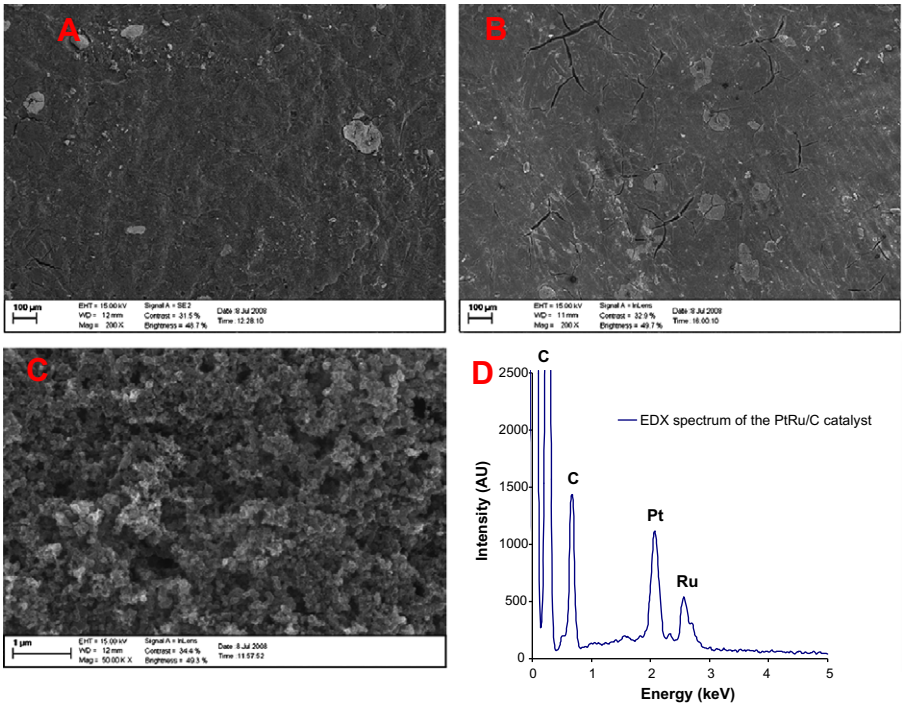

Fig. 9. Scanning Electron Microscopy of the PtRu/C catalyst: (A) Original PtRu/C catalyst surface observed at low magnification (×200); (B) PtRu/C catalyst surface after temperature treatment observed at low magnification (×200), highlighting the presence of cracks; (C) similar PtRu/C catalyst surface structure observed at high magnification (×50000); (D) EDX spectrum characteristic of the PtRu/C catalyst surface.

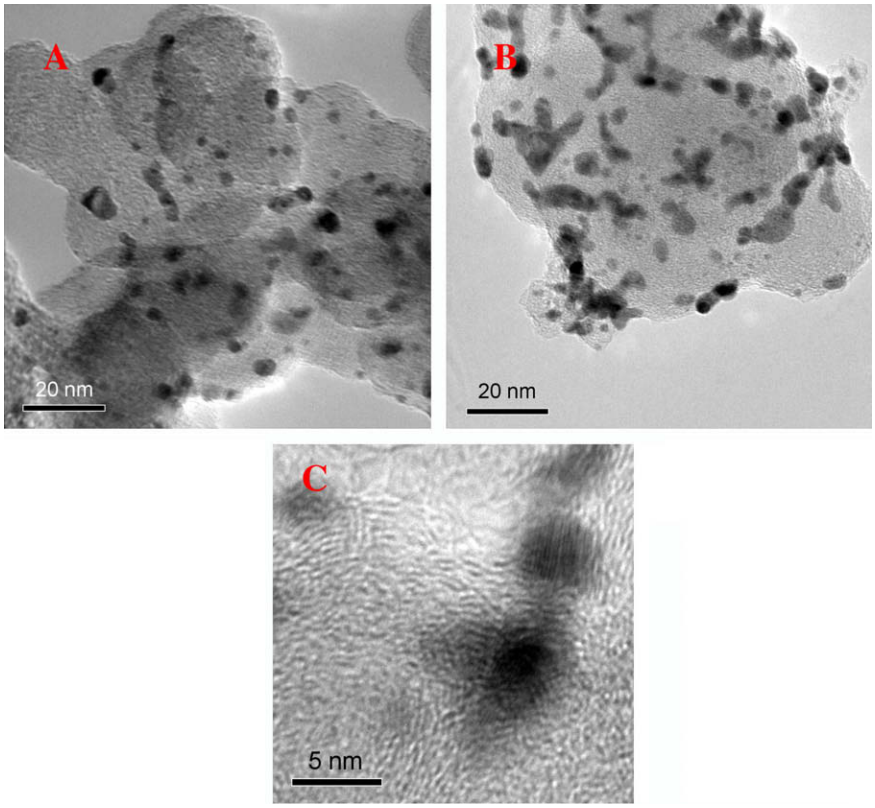

Fig. 10. Transmission Electron Microscopy of the PtRu/C catalyst: (A) Original PtRu catalyst nanoparticle observed at a ×230000 magnification; (B) PtRu catalyst nanoparticle after temperature treatment observed at a ×230000 magnification; (C) atomic structure of a PtRu catalyst nanoparticle observed at a ×880000 magnification.

Segregation within the PtRu particles may also happen, since it is known that Ru segregates to the surface of PtRu alloys in an oxidative environment, whilst Pt segregates to the surface in a reductive environment.

Acknowledgments

This work was carried out within the multi-annual programme of the European Commission's Joint Research Centre and with relation to the Framework Programme 6 (FP6) Specific Targeted Research Project (STREP) "FCAnode" (Non-noble Catalysts for Proton Exchange Membrane Fuel Cell Anodes). The authors would like to thank Jan van Eijk for the XRD measurements and Marc Steen for critical reading of the manuscript.

References

[1] G. Hoogers, D. Thompsett, CATTECH 3 (1999) 106.
[2] W. Vogel, J. Lundquist, P. Ross, P. Stonehart, Electrochim. Acta 20 (1975) 79.
[3] H. Igarashi, T. Fujino, M. Watanabe, J. Electroanal. Chem. 391 (1995) 119.
[4] P. Waszczuk, J. Solla-Gullon, H.-S. Kim, Y.Y. Tong, V. Montiel, A. Aldaz, A. Wieckowski, J. Catal. 203 (2001) 1.
[5] S.-Y. Huang, C.-M. Chang, C.-T. Yeh, J. Catal. 241 (2006) 400.
[6] S. Desai, M. Neurock, Electrochim. Acta 48 (2003) 3759.
[7] M.T.M. Koper, T.E. Shubina, R.A. van Santen, J. Phys. Chem. B 106 (2002) 686.
[8] T.E. Shubina, M.T.M. Koper, Electrochim. Acta 47 (2002) 3621.
[9] P. Liu, A. Logadottir, J.K. Norskov, Electrochim. Acta 48 (2003) 3721.
[10] H.A. Gasteiger, N. Markovic, P.N. Ross, E.J. Cairns, Surf. Sci. 98 (1994) 617.
[11] H.A. Gasteiger, P.N. Ross, E.J. Cairns, Surf. Sci. 293 (1993) 67.
[12] H.A. Gasteiger, N. Markovic, P.N. Ross, E.J. Cairns, Electrochim. Acta 39 (1994) 1825.
[13] H.A. Gasteiger, N. Markovic, P.N. Ross, J. Phys. Chem. 99 (1995) 8290.
[14] H.A. Gasteiger, N. Markovic, P.N. Ross, J. Phys. Chem. 99 (1995) 16757.
[15] J.C. Davies, B.E. Hayden, D.J. Pegg, Electrochim. Acta 44 (1998) 1181.
[16] J.C. Davies, B.E. Hayden, D.J. Pegg, Surf. Sci. 467 (2000) 118.
[17] J.C. Davies, B.E. Hayden, M.E. Rendall, D.J. Pegg, Surf. Sci. 496 (2002) 110.
[18] C. Roth, A.J. Papworth, I. Hussain, R.J. Nichols, D.J. Schriffin, J. Electroanal. Chem. 581 (2005) 79.
[19] Q. Ge, S. Desai, M. Neurock, K. Kourtakis, J. Phys. Chem. B 105 (2001) 9533.
[20] M.-S. Liao, C.R. Cabrera, Y. Ishikawa, Surf. Sci. 445 (2000) 267.
[21] Y. Ishikawa, M.-S. Liao, C.R. Cabrera, Surf. Sci. 513 (2002) 98.
[22] E. Christoffersen, P. Liu, A. Ruban, H.L. Skriver, J.K. Norskov, J. Catal. 199 (2001) 123.
[23] R.J. Behm, Acta Phys. Pol. A 93 (1998) 259.
[24] T. Kobayashi, P.K. Babu, J.H. Chung, E. Oldfield, A. Wieckowski, J. Phys. Chem. C 111 (2007) 7078.
[25] P.K. Babu, J.H. Chung, E. Oldfield, A. Wieckowski, Electrochim. Acta 53 (2008) 6672.
[26] H. Igarashi, T. Fujino, Y.M. Zhu, H. Uchida, M. Watanabe, Phys. Chem. Chem. Phys. 3 (2001) 306.
[27] J.C. Davies, G. Tsotridis, J. Phys. Chem. C 112 (2008) 3392.
[28] S.-C. Chang, M.J. Weaver, J. Chem. Phys. 92 (1990) 4582.
[29] M.W. Severson, C. Stuhlmann, I. Villegas, M.J. Weaver, J. Chem. Phys. 103 (1995) 9832.
[30] C.S. Kim, W.J. Tornquist, C. Korzeniewski, J. Chem. Phys. 101 (1994) 9113.
[31] C. Korzeniewski, J. Huang, Anal. Chim. Acta 397 (1999) 53.
[32] J. Huang, C. Korzeniewski, J. Electroanal. Chem. 471 (1999) 146.
[33] M. Andersen, M. Johansson, I. Chorkendorff, J. Phys. Chem. B 109 (2005) 10285.
[34] J.C. Davies, R.M. Nielsen, L.B. Thomsen, I. Chorkendorff, A. Logadottir, Z. Lodziana, J.K. Norskov, W.X. Li, B. Hammer, S.R. Longwitz, J. Schnadt, E.K. Vestergaard, R.T. Vang, F. Besenbacher, Fuel Cells 4 (2004) 1.
[35] J.C. Davies, J. Bonde, A. Logadottir, J.K. Norskov, I. Chorkendorff, Fuel Cells 5 (2005) 429.
[36] M. Heinen, Y.-X. Chen, Z. Jusys, R.J. Behm, ChemPhysChem 8 (2007) 2484.
[37] G. Ertl, M. Neumann, K.M. Streit, Surf. Sci. 64 (1977) 393.
[38] M. Xu, E. Inglesia, J. Phys. Chem. B 102 (1998) 961.
[39] P. Liu, J.K. Norskov, Fuel Cells 1 (2001) 192.
[40] P.A. Christensen, J.-M. Jin, W.-F. Lin, A. Hamnett, J. Phys. Chem. B 108 (2004) 3391.
[41] M. Iwase, S. Kawatsu, in: S. Gottesfeld, G. Halpert, A. Landgrebe (Eds.), Proceedings of the First International Symposium on Proton Conducting Membrane Fuel Cells, vols. 95-23, The Electrochemical Society, Pennington, NJ, 1995, p. 12.
[42] M.T.M. Koper, T.E. Shubina, R.A. van Santen, J. Phys. Chem. B 106 (2002) 686.
[43] M. Boudard, G. Djega-Mariadassou, Kinetics of Heterogeneous Catalytic Reactions, first ed., Princeton University press, New York, 1984.
[44] T. Matsushima, Surf. Sci. 79 (1979) 63.
[45] Z. Tang, D. Geng, G. Lu, J. Colloid Interf. Sci. 287 (2005) 159.
[46] P.K. Babu, H.S. Kim, S.T. Kuk, J.H. Chung, E. Oldfield, A. Wieckowski, J. Phys. Chem. B 109 (2005) 17192.
[47] T. Kobayashi, P.K. Babu, L. Gancs, J.H. Chung, E. Oldfield, A. Wieckowski, J. Am. Chem. Soc. 127 (2005) 14164.
[48] P.K. Babu, J.H. Chung, S.T. Kuk, T. Kobayashi, E. Oldfield, A. Wieckowski, J. Phys. Chem. B 109 (2005) 2474.
[49] K.S. Han, O.H. Han, P.K. Babu, J. Electrochem. Soc. 152 (2005) J131.
[50] S. Park, S.A. Wasilewski, M.J. Weaver, Electrochim. Acta 47 (2002) 3611.
[51] Z.B. Wang, G.P. Yin, P.F. Shi, Acta. Chim. Sin. 63 (2005) 1813.
[52] J. Wu, X.Z. Yuan, J.J. Martin, H. Wang, J. Zhang, J. Shen, S. Wu, W. Merida, J. Power Sources 184 (2008) 104.